Energy Nexus 5 (2022) 100030

Contents lists available at ScienceDirect

Energy Nexus

journal homepage: www.elsevier.com/locate/nexus

Impact of hydrodynamic conditions on optimum power generation in dual stage pressure retarded osmosis using spiral-wound membrane

Nahawand AlZainati[a], Sudesh Yadav[a], Ali Altaee[a,*], Senthilmurugan Subbiah[b], Syed Javaid Zaidi[c], John Zhou[a], Raed A. Al-Juboori[d,*], Yingxue Chen[e], Mohammad Hasan Shaheed[e]

[a] Centre for Green Technology, School of Civil and Environmental Engineering, University of Technology Sydney, 15 Broadway, NSW, 2007, Australia
[b] Department of Chemical Engineering, Indian Institute of Technology Guwahati, Guwahati, Assam 781039, India
[c] Department of Civil and Architectural Engineering, Qatar University, P.O. Box 2713, Doha, Qatar
[d] Water and Environmental Engineering Research Group, Department of Built Environment, Aalto University, P.O. Box 15200, Aalto, FI-00076 Espoo, Finland
[e] School of Engineering and Materials Science, Queen Mary University of London, London, E1 4NS, UK

ARTICLE INFO

Keywords:
Pressure retarded osmosis
Dual stage pressure retarded osmosis
Renewable energy
Salinity gradients
Power Generation

ABSTRACT

The Dual Stage Pressure Retarded Osmosis technique is considered for power generation. The influence of feed flow rates, hydraulic pressure, and pressure drop on mass transfer and solute diffusion in a full-scale membrane model was investigated for the first time to maximize power generation. Dead Sea-seawater, Dead Sea-reverse osmosis brine, reverse osmosis brine-wastewater, and seawater-wastewater salinity gradient resources were investigated for power generation. Results revealed a 71.07% increase in the specific power generation due to the dual-stage pressure retarded osmosis process optimization using Dead Sea-seawater salinity gradient resources. The increase in the specific power generation due to the dual-stage pressure retarded osmosis optimization was 108.8%, 63.18%, and 133.54%, respectively, for Dead Sea-reverse osmosis brine, reverse osmosis brine-wastewater, and seawater-wastewater salinity gradient resources. At optimum operating conditions, using the dual-stage pressure retarded osmosis process as an alternative to the single pressure retarded osmosis process achieved up to a 22% increase in the energy output. Interestingly, the hydraulic pressure at optimum operating conditions was slightly higher than the average osmotic pressure gradients in the dual-stage pressure retarded osmosis process. The study also revealed that power generation in the dual-stage pressure retarded osmosis process operating at constant mass transfer and solute resistivity parameters was overestimated by 2.8%.

1. Introduction

Sustainable energy is acquired from everlasting sources; these sources are naturally reproduced, such as wind, solar, geothermal heat, biomass and hydropower. The most significant attribute for renewable energy, being clean, is infinite. It has much lower negative impacts on the environment compared to conventional fossil energy [1]. Further, productizing and capitalising on renewable energy sources would improve the world's energy security, lower the conventional fuels price, and save fossil fuel reserves for future generations. It would also reduce pollution and present a possibility to minimize greenhouse gas emissions to levels that will settle down greenhouse gases in the atmosphere. It might also decrease the reliance on imported fuels, support economic development, and offer new jobs [2]. Pressure Retarded Osmosis (PRO) is considered a potential source of sustainable energy, and it is found to be higher power density and more efficient than reverse electrodialysis [3]. It is the process that produces hydraulic pressure from the osmotic pressure of a saline mixture.

A colossal power is available in the earth's waters due to the variance in the salinity of freshwater and seawater. Annually and worldwide, there are around 37,300 km^3 discharged from rivers water. Mixing this amount of water with seawater could produce around 2 TW of renewable energy. The pressure Retarded Osmosis (PRO) process is one methodology that can be considered to gather the power obtainable of salinity gradient resources (SGRs). Unlike other renewable energies affected by solar irradiation and wind variation, pressure retarded osmosis employs membrane technology for power generation from a pair of solutions of different salinity concentrations, which is not affected by weather conditions [4].

The concept of using stages in the pressure retarded osmosis (PRO), such as dual-stage pressure retarded osmosis (DSPRO), has demonstrated the capability of increasing the generated energy from salinity

* Corresponding authors.
E-mail addresses: ali.altaee@uts.edu.au (A. Altaee), Raed.Al-juboori@aalto.fi (R.A. Al-Juboori).

https://doi.org/10.1016/j.nexus.2021.100030
Received 15 October 2021; Received in revised form 4 November 2021; Accepted 28 November 2021
Available online 2 December 2021

Nomenclature

Symbol	
DSPRO	Dual Stage Pressure Retarded Osmosis
DS-SW	Dead Sea-Sea Water
DS-ROB	Dead Sea- Reverse Osmosis Brine
ROB-WW	Reverse Osmosis Brine-Waste Waters
SW-WW	Sea Water-Waste Water
SGRs	Salinity Gradient Resources
PRO	Pressure Retarded Osmosis
CP	Concentration Polarization
DS	Draw Solution
FS	Feed Solution
ΔP	Applied hydraulic pressure difference
$\Delta\pi$	Osmotic Pressure difference
Aw	The water permeability in L/m^2.h.bar
B	The salt permeability in L/m^2.h.bar
S	The membrane structural parameter in μm
k_d	The mass transfer coefficient in m/h
Sh	Sherwood number
D	The diffusion coefficient in m^2/s at 20°C
d_h	The hydraulic diameter in m
Re	Reynold number
Sc	Schmidt number
ρ_D	The draw solution density in Kg/m^3
V	The draw solution velocity in m/s
μ	The viscosity of the draw solution in kg/m.s at 20 °C
X_{NaCl}	The mass fraction of the salt in the draw solution
X_{H2O}	The mass fraction of the water in the draw solution
Q	The solution flow rate in L/h
As	The cross-section area of the membrane in m^2
A	The membrane surface area in m^2
D_{T2}	The diffusion coefficients in m^2/s at 25°C
K	The solute diffusion resistivity in h/m
D_F	The diffusion coefficient at the support layer in m^2/s at 20°C
n	The number of the ions in solution
R	The universal gas constant in J/mol.K
C	The stream molar concentration in M
P	The hydraulic pressure in bar
W	Power density in W/m^2
Eo	The specific power generation in kWh/m^3
Eo_tot	The specific power generation in the entire system in kWh/m^3

The subscripts	
i	Used for the inlet parameters
o	Used for the outlet parameters
T	Temperature of 20°C (293 K)
T2	Temperature of 25°C (298 K)
j	Represents the stage number (j = 1 for the first DSPRO stage and j = 2 for the second DSPRO stage)
F	Used for feed solution
D	Used for draw solution
x	Represents the distance along the membrane in m
1	Represents the first DSPRO stage
2	Represents the second DSPRO stage

gradient resources (SGRs) [5,6]. Adding another stage to the PRO process recovers the residual osmotic power in the less concentrated draw stream before exiting the first PRO stage [4–7]. In the DSPRO process, a portion of the diluted draw stream equals the permeate flow rate in stage one of the process and goes to stage two (Fig. 1). A new feed stream is entered to the second DSPRO stage to rejuvenate the chemical potential by reducing the feed side concentration polarization (CP) [6,8].

A recent study exhibited that power generated from the PRO process could be elevated by 18% when a second stage is added [4]. An improvement of up to 8% in the specific energy was noticed in research when the DSPRO system was utilized instead of a single PRO process [4]. Altaee et al. [6] proposed that the maximum power generation for Dead Sea-reverse osmosis brine (DS-ROB) SGR showed 16% enhancement due to adding a second PRO stage. Another study investigating the PRO membrane arrangement in the DSPRO process revealed that the highest specific power generation was when two PRO modules were used in stage one and one module in the second stage [6]. The study assumed an operating pressure of 50% of the osmotic pressure difference ($\Delta P=\Delta\pi/2$), and the draw to feed solution flow rate ratio is equal to one. These optimum conditions in laboratory-scale systems are not valid in the PRO process using a full-scale module owing to the simultaneous dilution of the draw solution (DS) and concentration of the feed solution (FS) along the PRO module [9]. As a matter of fact, power generation could be increased by ~54% due to optimizing the hydrodynamic parameters, i.e. flow rates and hydraulic pressure [9]. Unfortunately, there is no study yet, investigating power generation in the DSPRO, considering the impact of hydrodynamic parameters on the coefficients of mass transfer and solute resistivity to diffusion.

Soltani and Struchtrup [8] showed a preferable performance of the DSPRO over a single PRO process. The study examined changes in hydraulic pressure, flow rates, and feed concentrations through the membrane length, but it assumed that hydrodynamic parameters were constant along the membrane. Another study performed by He et al. [5] confirmed that including a second stage in the PRO process would increase the energy harvested from the salinity gradient. The study did optimize the main operating conditions, but it did not investigate the changes in the draw and feed streams concentrations in a full-scale module. The PRO process was also investigated under theoretical basis and optimization of extractable osmotic power from a brine solution, proposing a model-based optimization to maximize the normalized specific energy production (NSEP) [10]. In this study, the power generation from a counter-current and constant pressure DSPRO has taken place by applying dimensionless parameters in the simulation model, considering the membrane characteristics and feeds and operating conditions. The study outcomes demonstrated that the multistage PRO process is more productive than a single-stage PRO [10]. Nevertheless, the study ignored the pressure drop and did not include the CP effect. Altaee et al. [11] also showed the superiority of DSPRO over a single-stage PRO in their study; however, the study did not evaluate the effect of flow rate and applied pressure in the PRO module. In 2013, a full-scale module (hollow-fibre) was employed in a PRO pilot plant process [12]. The power density was 4.4 W/m^2 from a 4.7% sodium chloride RO brine-sewage solution salinity gradient with equal feed stream flow rates. The work overlooked the influence of the applied pressure and the flow rate ratio of the feed to the draw solution on the pilot plant performance. In another PRO pilot plant study [13], a power density of 7.7 W/m^2 was attained utilizing RO brine-wastewater salinity gradient and Toyobo hollow fibre membrane. However, the study did not consider the effect of feed and draw solutions flow rates on the process productivity. A PRO process with a full-scale module was optimized by a machine learning algorithm based on non-ideal operating parameters [14]. The study demonstrated that power generation maximized at an applied pressure lower than $\Delta P=\Delta\pi/2$. Nevertheless, the study did not consider the changes in mass transfer and solute resistivity through the membrane length.

It has also been noticed that only a few studies focused on the DSPRO modelling [15,16], despite that, no studies are available to define the optimum hydraulic pressure, the ratio of the inlet flow rates, and the pressure drop in both sides of a full-scale PRO module. Moreover, several studies in the literature did investigate the impact of utilizing higher draw and feed flow rates in the process. Recently Habtom et al. [17] studied the importance of optimizing the operating parameters and module dimensions in the PRO process to achieve maximum energy output from seawater-river water SGR. Also, the study concluded that the

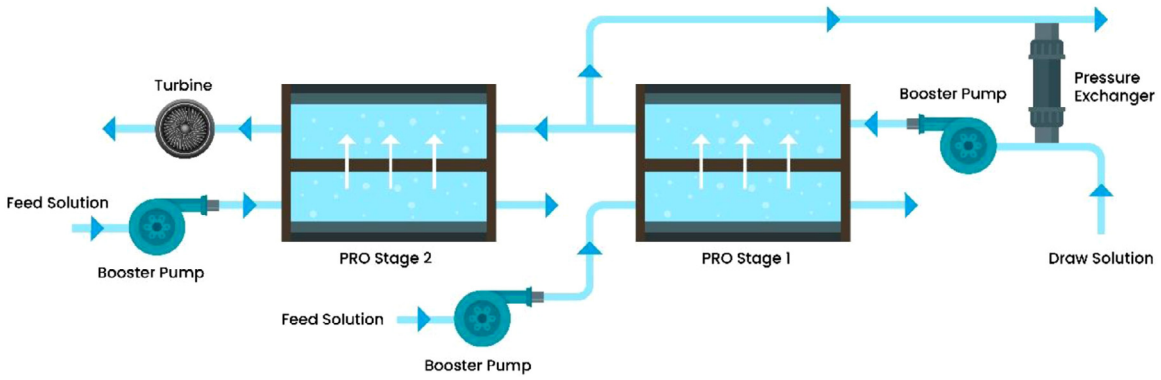

Fig. 1. Illustration figure of DSPRO process for power generation from SGRs, where the SGRs as draw solution-feed solution can be Dead Sea-Sea water, Dead Sea-Reverse Osmosis brine, Reverse Osmosis brine-Wastewater or Sea water-Wastewater, respectively.

optimization of the PRO process is based on power density or might cause a suboptimal solution for the PRO-ERD integrated system. Still, the optimum hydrodynamic parameters of PRO and DSPRO processes for various salinity gradient resources are not reported in the literature [11,18,19]. Regardless of that, some studies considered optimizing bench-scale PRO processes [20,21], but there is no study available to optimize a DSPRO.

Herein, this study investigated the optimum operating parameters in the DSPRO using a full-scale module, considering the influence of the feed stream flow rates on solute resistivity and mass transfer conditions in the PRO module. The latter parameters are a function of solution concentration which varies along the PRO module. In addition, the pressure drop on both solutions sides of the membrane was taken into account. To the extent of our knowledge, no research has been performed to date, investigating the variations of the hydrodynamic parameters along the PRO membrane. Four different SGRs were investigated in the current work, i.e. 5M-0.6 M, 5M-1.2 M, 1.2M-0.02 M, and 0.6M-0.02 M, to understand the influence of the feed and the draw solutions concentrations on the process productivity and hydrodynamic operating conditions. These SGRs are widely investigated in literature and available in the environment, representing Dead Sea-Sea water (DS-SW), Dead Sea-Reverse Osmosis brine (DS-ROB), Reverse Osmosis brine-Wastewater (ROB-WW), Sea water-Wastewater (SW-WW), respectively.

2. Methodology

2.1. Spiral-Wound FO membrane characteristics

Since there is no spiral wound PRO membrane available now, this study assumed that the PRO membrane would have the same characteristics of commercial spiral wound cellulose triacetate (CTA) membrane fabricated by Hydration Technology Innovation Company (HTI). The HTI membrane series OsMem 8040FO-FS-P was investigated for power generation, assuming it would tolerate elevated hydraulic pressures [22]. The active membrane area is 16.5 m^2, module length is 1.0 m, the feed temperature is 20 °C, and the number of membrane leaves is 11. The coefficient of water permeability (Aw), salt permeability (B), and the structural parameter (S) are 0.76 L/m^2.h.bar, 0.44 L/m^2.h and 655 μm, respectively [22].

2.2. The mass transfer and solute diffusion resistivity coefficient

The mass transfer coefficient (k_d) varies along the membrane length (e.g. at every x (m) distance of the membrane) as the draw flow rate, *Re* number, the draw stream concentration, and diffusivity varies along the membrane length. k_d, was determined by the following equations:

$$k_d = Sh * D/d_h \quad (1)$$

The hydraulic diameter of the flow through the feed spacer is equal to double the feed spacer thickness (2 × 0.0025 = 0.005 m). The flow has been assumed turbulent at all flow rates, and under that condition, Sh number can be found by the following expression:

$$Sh = 0.2Re^{0.57}Sc^{0.40} \quad (2)$$

where *Re* and *Sc* are the Reynold and the Schmidt number, respectively. The Reynolds number is calculated using Eq. (3).

$$Re = \rho_D V d_h/\mu \quad (3)$$

The draw solution viscosity was calculated at each concentration at 20 °C and 25°C by interpolating data from literature [23]. The density of the draw solution was calculated based on Eq. (4).

$$\rho_D = \frac{1}{\left(\frac{X_{NaCl}}{\rho_{NaCl}}\right) - \left(\frac{X_{H2o}}{\rho_{H2o}}\right)} \quad (4)$$

The solution velocity is calculated as:

$$V = Q_{Di,x}/A_s \quad (5)$$

In equation [5], A_s is the cross-section area of the membrane, which is equal to the multiplication of the thickness of the spacer (0.0025 m) by the width of the channel (0.66 m); A_s = 0.00165 m^2. Next, the Schmidt number (*Sc*) can be given by the following equation:

$$S_c = \frac{\mu}{\rho_D D} \quad (6)$$

The diffusivity of NaCl at different concentrations at 25 °C was found by interpolating data found in the literature [24]. These values were used to calculate the diffusivity of the draw solutions at 20 °C as follows:

$$\frac{D}{D_{T2}} = \frac{T}{T_2}\frac{\mu}{\mu_{T2}} \quad (7)$$

After finding D at 20°C, *Sc*, Sh, and k_d can be calculated at every 0.1 m of the membrane length.

The solute diffusion resistivity (K) will vary along the PRO module due to the variations in the viscosity of the FS, and the following equation calculates it:

$$K = \frac{S}{D_F} \quad (8)$$

DS-SW, DS-ROB, ROB-WW, and SW-WW SGR were investigated to cover a variety of feed and draw solutions concentrations, regardless of the osmotic energy and the power generated by these salinity gradients.

2.3. The numerical model of PRO

Water flux was predicted in both DSPRO stages using a mathematical model developed by Ali et al. [25], that considers the effect of concentration polarization and the external resistivity on the support layer, as

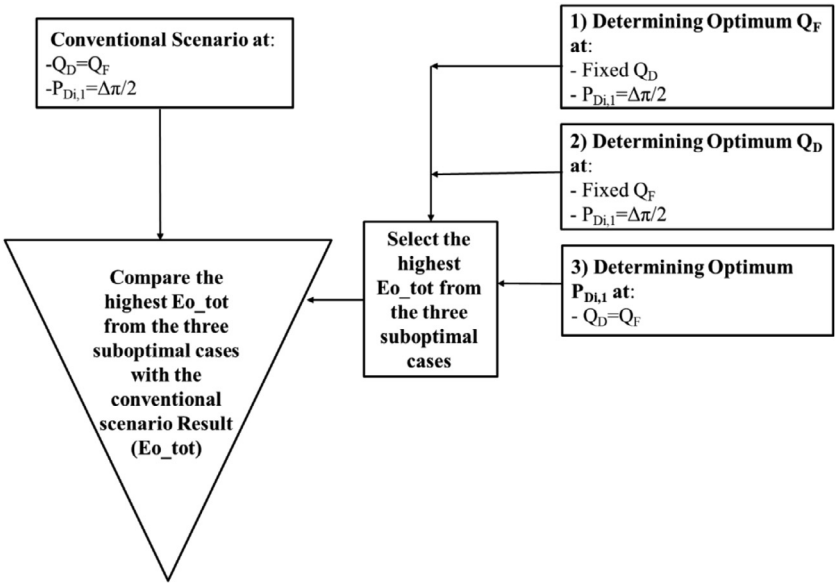

Fig. 2. Schematic representation of the systematic simulation of DSPRO system for process optimization, three suboptimal cases were considered to determine the optimum operating parameters. The highest specific power generation from the three cases is compared with the corresponding one in the conventional scenario.

shown in the following equation:

$$J_{w,x} = A_w \left(\frac{\left(\frac{nRTC_{Di,x}\left(1+\frac{Q_{Di,x}}{Q_{Do,x}}\right)}{2} \right) \exp\left(\frac{-J_{w,x}}{k_{d,x}}\right) - \left(\frac{nRTC_{Fi,x}\left(1-\frac{Q_{Fi,x}}{Q_{Fo,x}}\right)}{2} \right) \exp\left(J_{w,x}K_x\right)}{1 + \frac{B}{J_{w,x}}\left(\exp\left(J_{w,x}K_x\right) - \exp\left(\frac{-J_{w,x}}{k_{d,x}}\right)\right)} - \Delta P_x \right) \quad (9)$$

In Eq. (9), ΔP_x is $((P_{Di,x}-\Delta P_{D,x})-(P_{Fi,x}-\Delta P_{F,x}))$. This model is used to determine the permeation flux value in the two DPRO stages. k_d and K were changing along the membrane length. It has been presumed that the pressure exchanger efficiency is 98%, and the solute leakage in the pressure exchanger is neglected. The specific power generation ($Eo_{x,j}$) along the two DPRO stages was calculated, as shown in Eq. (10).

$$E_{ox,j} = \frac{\Delta P_{x,j} * Q_{Px,j}}{Q_{Di,j} + Q_{Fi,j}} \quad (10)$$

Where $\Delta P_{x,j}$ ($(P_{Dix,j}-\Delta P_{Dx,j})-(P_{Fix,j}-\Delta P_{Fx,j})$) is the effective pressure variance between the draw and feed streams at distance x in j DPRO stage through considering the pressure drop at the draw ($\Delta P_{D,xj}$) and the feed side ($\Delta P_{Fx,j}$) and $Q_{Px,j}$ is the permeate flow rate at distance x in the membrane module. In the second DPRO stage, the feed and draw flow rates equal the permeate flow rate in stage one ($Q_{Di,2}$=$Q_{Fi,2}$=$Q_{P,1}$). The membrane area in the second DSPRO stage can be correlated to the first and second stage flow rate of the draw solution and the membrane area of the first DSPRO stage, and it was calculated as follows:

$$A_2 = A_1 * \frac{Q_{Di,2}}{Q_{Di,1}} \quad (11)$$

The sum of the specific power generation in both DSPRO stages equals the net specific power generation. More details about the water flux can be found in the literature [26]. The built MatLab Code did all of the previous calculations at every x (m) of the membrane length. The systematic simulation-based optimization study of the DSPRO was done by varying the main operating parameters: the draw flow rate, the feed flow rate, and the applied hydraulic pressure [18,20]. The study of determining the optimum parameters of the DSPRO is divided into three main parts (suboptimal cases) (Fig. 2), where the results from all cases are compared to the conventional scenario:

i Determining the optimum feed flow rate (Q_F) at fixed Q_D and $P_{Di,1}$=Δπ/2
ii Determining the optimum draw flow rate (Q_D) at fixed Q_F and $P_{Di,1}$=Δπ/2
iii Determining the optimum $P_{Di,1}$ at constant Q_D=Q_F

In each scenario, various pressure values or various flow rates were assumed. The specific power generated was calculated for the four different sets of SGRs. In the end, the maximum specific power generated was compared with the specific power generated by the conventional DSPRO process. The parameter that governs the productivity of the DSPRO process in the current study is the produced specific power. The three cases will demonstrate which parameter is the most dominant on the DSPRO performance. Eqn. (1)–8

2.4. The model validation

The experimental data performed by Achilli et al. [27] on a laboratory-scale FO membrane is considered in this study to validate the model of water flux. In the experimental study, 18.75 cm^2 is the flat-sheet membrane area, A_w is 6.7×10^{-4} m/h bar, B is 4×10^{-4} m/h, the membrane module length is 75 mm, S is 800 μm, k_d is 0.306 m/h, and K is 125.27 h/m [27]. The feed solution concentration in the experimental study is between 0 and 5 g/L, while the draw solution concentration is 35 and 60 g/L. The applied pressure ranged from 11 to 24 bar (Table 1), with a 0.5 L/min flow rate for the draw and the feed solutions [27]. The agreement percentage is calculated as 100% minus the error percentage. The error percentage is the absolute difference between the model output (water flux or power density) and the experimental output divided by the experimental output. Results show a significant agreement, over 89% compatibility, between the experiment and the model (Table 1).

2.5. Pressure drop calculations

The pressure drop on the feed and draw sides was calculated. Eq. (12) was suggested by the HTI company to calculate the pressure drop in the feed stream at 20°C:

$$\left[0.097 * \left(Q_{Fi,1} in\ LPM/(total\ leaves)\right) + 5.9\right] * \left(Q_{Fi,1} in\ LPM/(total\ leaves)\right) = \Delta P_F (in\ kPa/element) \quad (12)$$

The pressure drop from Eq. (12) represents the pressure drop in one membrane module. To find the pressure drop in the feed side at every 0.1 m of the membrane length, the value from Eq. (12) is multiplied by 0.1 since the length of the membrane is 1.0 m with 10 sections of 0.1 m

Table 1
The percentage agreement between the water flux and the power density of the experimental results, [27] and the model used in the current study.

Draw Concentration (g/L)*	Feed concentration (g/L) *	Pressure (bar) *	Water flux-Experimental (LMH) *	Water flux-Model (LMH)	%Water flux agreement	Power density-Experimental (W/m^2) *	Power density-Model(W/m^2)	%Power densityagreement
35	0	13	7.9	8.8	89%	3.1	3.4	90%
	2.5	12	6.8	6.8	100%	2.3	2.5	91%
	5	11	5.6	5.5	98%	1.8	1.8	100%
60	0	24	12.4	12.8	97%	8.9	8	90%
	2.5	23	10.1	9.9	98%	6.2	6.6	94%
	5	22.5	8.5	8.1	95%	4.8	5.2	92%

* parameters are from reference [27].

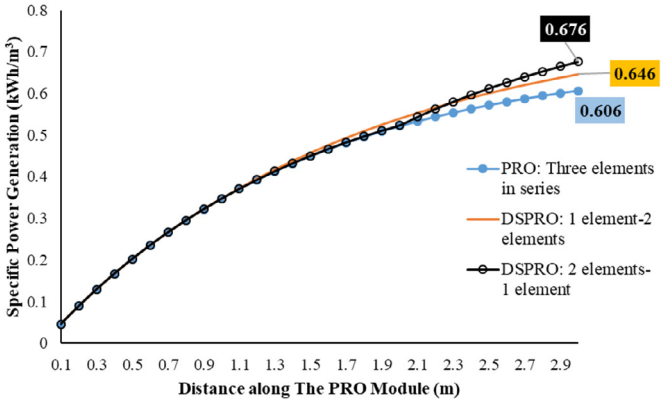

Fig. 3. The specific power generation along the membrane module of a PRO system of three elements in series and two configurations of a DSPRO system (1element in stage one-2 elements in stage two, and 2 elements in stage one-1 element in stage two). The feed and the draw solutions flow rates are 500 L/h, 5M-0.6 M NaCl are the salinity gradient sources, and the hydraulic pressure is half of the osmotic pressure.

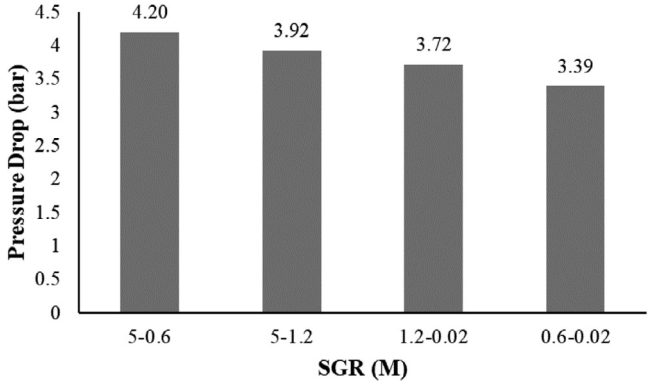

Fig. 4. The pressure drop of the DSPRO process includes two membrane modules in stage one and one membrane module in stage two of equal feed's flow rates (1000 L/h) and hydraulic pressure of half of the osmotic pressure difference for various SGRs.

each. On the draw stream, the pressure drop at 20 °C was calculated from Eq. (13):

$$95 * \left[Q_{Di,1} in\ LPM/(total\ leaves)\right] = \Delta P_D (in\ kPa/element) \quad (13)$$

Likewise, the pressure drop in the draw side was calculated at every 0.1 m of the membrane by multiplying the pressure drop value from Eq. (13) by 0.1. Eqs. (12) and 13 calculate pressure drop at 20 °C. Also, pressure drops from Eqs. (12) and 13 are multiplied by the solution viscosity at 20 °C when different concentrations are used.

3. Results and discussions

3.1. PRO membranes arrangement in the vessel

The effect of the membrane arrangement on the DSPRO performance is investigated with 5M-0.6 M SGR, representing the DS-SW salinity gradient often used in the PRO process [6]. Previous studies suggested three PRO elements to evaluate the specific power generation at different membrane arrangements [6]. In practice, water flux drops significantly at the end of the third PRO element; hence, adding a fourth PRO element will not generate tangible permeation flow to impact the performance of the PRO process. Also, the HTI pressure vessel accommodates up to three elements. Considering these technical limitations, the following DSPRO membrane configurations were simulated (Fig. 3) i) three modules in a single PRO stage ii) DSPRO system with one module in stage one and two modules in stage two, and iii) the third DSPRO configuration suggests two modules in sage one and one module in stage two. It should be noted that the PRO and the DSPRO process use an equal membrane area, i.e. three membranes in the vessel.

The draw solution pressure is half of the osmotic pressure of the DS-SW salinity gradient ($\Delta P = \Delta\pi/2$), and each module is 1 m long, with 16.5 m^2 active membrane area. The specific power generation was calculated for each case and used to identify the best performance configuration. As shown in Fig. 3, the PRO system with three modules in series had the lowest specific power generation (0.606 kWh/m^3) compared to the other configurations. Using a DSPRO system with one module in stage one and two modules in stage two achieved 0.646 kWh/m^3, i.e. greater than three membrane modules in series. The maximum power generated (0.676 kWh/m^3) occurred at the DSPRO system with two modules in stage one and one module in stage two, and hence this configuration was selected in this study. The findings are consistent with the previous study by Alanezi and Altaee [15], where the DSPRO system performed better when configured as two modules in stage one and one module in stage two.

3.2. Pressure drop in the module

The pressure drop in the HTI membrane was calculated at the feed and the draw stream sides at 0.1 m distance along the module. Eqs. (12) and 13 show that mass transfer across the membrane will influence the pressure drop of the PRO membrane. Technically, the hydrodynamic conditions of the feed and the draw solutions change due to the permeation flow, affecting the pressure drop in the PRO membrane. Equal flow rates of the draw and the feed solutions (1000 L/h) were utilized to determine the pressure drop along the membrane modules in the DSPRO process and $\Delta P = \Delta\pi/2$. For instance, the pressure drop at the end of the third PRO module for 5M-0.6 M was a 4.2 bar, as shown in Fig. 4. The results show a higher pressure drop in the SGRs of higher osmotic pressure gradients. The pressure drop for the 5M-0.6 M was slightly higher than the other SGRs as a result of the higher permeation flux and flow rate along the PRO module.

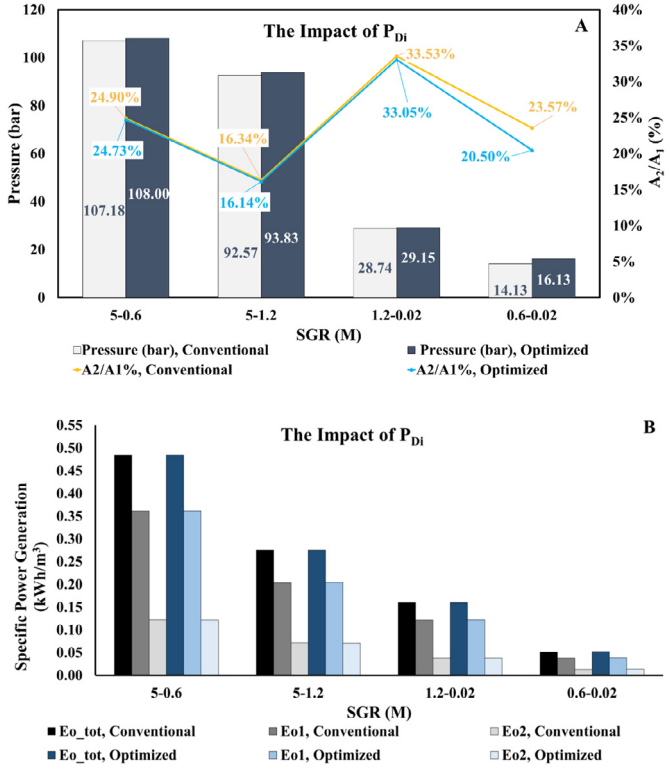

Fig. 5. The effect of the optimum hydraulic pressure of the DSPRO process on the specific power generation for various SGRs. A) the conventional and optimized hydraulic pressure and the conventional and optimized membrane area ratio (A_2/A_1%) for all SGRs. B) Specific power generation in the conventional and optimized DSPRO processes for the used SGRs at stage one (Eo1), stage two (Eo2), and the total amount at both stages (Eo_tot).

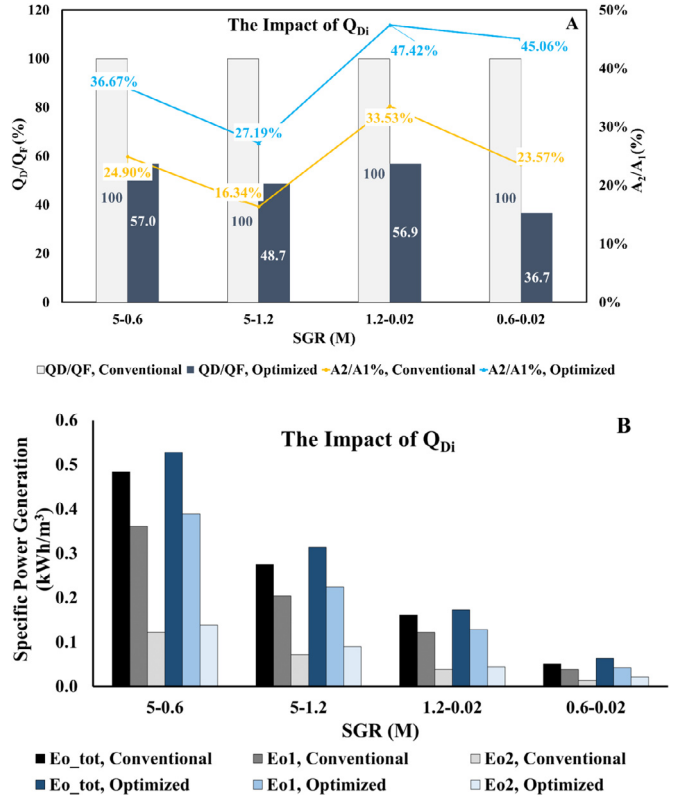

Fig. 6. The effect of DSPRO optimum draw solution flow rate on the specific power generation for various SGRs. A: the conventional and optimized ratio of Q_D/Q_F% and conventional and optimized A_2/A_1% for the four SGRs. B: Specific power generation in the conventional and optimized DSPRO processes for the SGRs at stage one (Eo1), stage two (Eo2), and the total amount at both stages (Eo_tot).

3.3. Determining the optimum hydraulic pressure

Previous laboratory-size studies pointed out that the optimum hydraulic pressure of $\Delta P=\Delta\pi/2$ is not applicable for large-scale systems [11,14]. Accordingly, this work investigated the impact of the hydraulic pressure on the power generation to find the optimum hydraulic pressure (PDi,1) at a 1000 L/h flow rate for the draw and feed solutions. It is worth mentioning that 1000 L/h is within the flow rate recommended by the HTI Company. The membrane area on the second stage was calculated using Eq. (11).

Results indicated that the optimum hydraulic pressure of the optimized DSPRO process is slightly higher than $\Delta\pi/2$ for all SGRs (Fig. 5A). The optimum hydraulic pressure was 0.76%, 1.36%, 1.41, and 14.16% higher than $\Delta\pi/2$ for 5M-0.6 M, 5M-1.2 M, 1.2M-0.02 M, and 0.6M-0.02 M SGR, respectively. The results disagree with previous studies findings and suggest that the optimum hydraulic pressure in a full-scale module is less than $\Delta\pi/2$ [28]. This disagreement can be justified since previous studies did not consider the pressure drop in the PRO process or the change in mass transfer. Fig. 5A also shows a higher membrane area in the second stage, i.e. A_2/A_1 ratio, in the conventional DSPRO processes that operates at lower hydraulic pressure due to higher water flux than in the DSPRO working at optimum pressure (Appendix A Fig. A1). The ratio of A_2/A_1 in the conventional DSPRO was between 16.34% and 33.53%, while it was between 16.14% and 33.05% in the processes operating at optimum pressure.

The specific power generation was calculated for optimized and conventional DSPROs (Fig. 5B). The specific power production was calculated in stage one (Eo1), stage two (Eo2), and the entire process (E_tot). In stage one, the results showed a slight increase in the specific power generation in the DSPRO process operated at optimum applied pressure compared to the conventional DSPRO process, probably, due to the higher draw solution pressure in the former process. In stage two, Eo2 in the DSPRO process at optimum applied pressure was lower than in the conventional DSPRO process for 5M-0.6 M, 5M-1.2 M, and 1.2M-0.02 M SGRs and higher for 0.6M-0.02 M SGR (Fig. 5A). The reduction in Eo2 for 5M-0.6 M, 5M-1.2 M, and 1.2M-0.02 M is attributed to the serious CP in the first stage, which reduced the permeation flow, hence the flow rates of the draw stream entering the second stage, leading to a decrease of Eo2. The effect of concentration polarization in 0.6M-0.02 M was inadequate due to the low water flux produced by these solutions. Hence, the Eo2 was slightly higher in the DSPRO process operating at optimum pressure.

The total specific power (Eo_tot) was between 0.007% and 2.45% higher in the DSPRO process operating at optimum hydraulic pressure, and the highest increase was for 0.6M-0.02 M. Generally, using optimum hydraulic pressure caused only a slight increase in Eo_tot. Compared to a single-stage PRO process, using DSPRO process brought about 33.8%, 35%, 31% and 34.7% increase in Eo_tot for 5M-0.6 M, 5M-1.2 M, 1.2M-0.02 M, and 0.6M-0.02 M, respectively.

3.4. Determining the optimum draw flow rate

The flow rate of the draw solution is a critical parameter that impacts the DSPRO processes' efficiency [5,26]. Determining the optimum value of the draw solution flow rate in the DSPRO process was performed at $P_{Di,1}=\Delta\pi/2$, and $Q_{Fi,1}$ = 1000 L/h. The flow rates ratio in the first DSPRO stage (Q_D/Q_F) and the membrane areas ratio (A_2/A_1) for the optimized and conventional DSPRO processes are shown in Fig. 6A. The optimum ratio of Q_D/Q_F was different for each SGR. For instance,

the optimum Q_D/Q_F ratio was 57% for 5M-0.6 M, 48.7% for 5M-1.2 M, 56.9% for 1.2M-0.02 M, and 36.7% at 0.6M-0.02 M. The Q_D/Q_F is governed by the water flux influenced by the concentration polarization in membrane processes. For example, Q_D/Q_F ratio 5M-0.6 M was higher than in 5M-1.2 M salinity gradient as a result of the greater permeation flux in the former salinity gradient that required an increase in the flow rate of the draw solution to reduce the dilutive CP. Likewise, the lowest Q_D/Q_F ratio was the 0.6M-0.02 M SGR that exhibited low water flux.

The percentage of A_2/A_1 in Fig. 6A shows differences in the membrane areas required in the optimized and the conventional DSPRO processes. For example, the A_2/A_1 ratio in the 0.6M-0.02 M was 45.06% and 23.57% in the optimized and conventional DSPRO processes, respectively. A 91.17% increase in the A2/A1 in the optimized process is due to the lower $Q_{Di,1}$ in the first stage of the optimized DSPRO process. According to Eq. (11), A_2 is a function of $Q_{Di,1}$ and $Q_{Di,2}$, but it is more affected by $Q_{Di,1}$. On the contrary, for the 5M-0.6 M SGR, A_2 increased by 47.25% in the DSPRO process operated at optimum draw solution flow rate compared to the conventional process due to the lower $Q_{Di,1}$ of the optimized process, which confirms the finding mentioned above. A_2/A_1 ratios were between 16.34% and 33.53% in the conventional processes and 27.19% and 47.42% in the DSPRO at optimum draw solution flow rates.

The specific power generation was calculated for all SGRs at optimum draw solution flow rates and compared with the conventional processes (Fig. 6B). The Eo_tot was 9.1%, 13.93%, 8.05%, and 24.22% higher for salinity gradients 5M-0.6 M, 5M-1.2 M, 1.2M-0.02 M, and 0.6M-0.02 M, respectively, in the DSPRO process operating at the optimum Q_D. At optimum Q_D, there was between 5% and 12% increase in the Eo1 and between 13% and 61% in the Eo2. Using optimum Q_D caused an increase in Eo1 and Eo2 due to the lower Q_D in the DSPRO process (Eq. (10)). The effect of using the optimal draw flow rate on process performance was significantly greater than the effect of using the optimal hydraulic pressure. The specific power generated improved by 9.1% to 24.22% after determining the optimum Q_D, but it was 0.007% to 2.45% after determining the optimum hydraulic pressure. The results also revealed an enhancement in Eo_tot between 35.6% and 49.4% when including a second PRO stage to the DPSRO process in comparison to a single-stage PRO process.

3.5. Determining the optimum feed flow rate

The flow rate of the feed solution is another important parameter that affects DSPRO performance. The optimum feed flow rate and its impact on the power generation were performed at $P_{Di,1} = \Delta\pi/2$ and $Q_{Di,1}$ = 1000 L/h. Fig. 7 shows Q_F/Q_D ratio, A_2/A_1 ratio, and Eo_tot of the optimized and conventional DSPRO processes. Results show that the optimized DSPRO required lower Q_F/Q_D ratios than the conventional DSPRO (Fig. 7A). The Q_F/Q_D ratios for the optimized processes were 28%, 42.4%, 27.8% and 25.8% for 5M-0.6 M, 5M-1.2 M. 1.2M-0.02 M, and 0.6M-0.02 M, respectively. The highest optimum flow rates ratio (Q_F/Q_D) was 42.4% for 5M-1.2 M, which is expected as the feed concentration is the highest compared to other SGRs. Internal CP has a greater effect as feed concentration increases, and thus a high feed solution flow rate is required to minimize concentrative CP. [29]. The severity of the concentrative CP for 1.2M-0.02 M and 0.6M-0.02 M is lower than the other SGRs due to the low feed concentration. Consequently, the Q_F/Q_D values were lower for 1.2M-0.02 M and 0.6M-0.02 M. In effect, the Q_F and the ratio of Q_F/Q_D are governed by the feed concentration; the lower the feed concentration, the lower the feed solution flow rate is required.

Fig. 7A also shows the A_2/A_1 ratio of the optimized and conventional DSPRO processes. Contrary to the optimum Q_D, the A_2/A_1 ratios were less in the optimized DSPRO processes than the conventional ones. The A_2/A_1 ratios for the conventional processes were 24.9%, 16.34%, 33.53% and 23.57% for 5M-0.6 M, 5M-1.2 M. 1.2M-0.02 M, and 0.6M-0.02 M, respectively. The corresponding results for the optimized DSPRO processes were 20.76%, 13.88%, 26.42%, and 21.45%

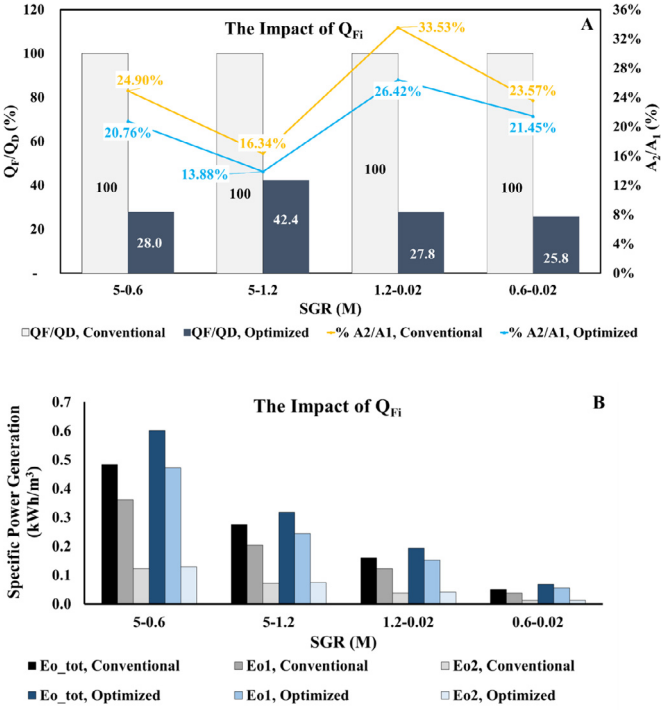

Fig. 7. Impact of the optimum feed solution flow rate on the specific power generation for various SGRs. A) the conventional and optimized ratio of the feed solution flow rate to the draw solution flow rate in the first DSPRO stage (Q_F/Q_D%) and the conventional and optimized membrane area ratio (A_2/A_1%) for the four SGRs. B) (Eo1), (Eo2), and (Eo_tot) in the conventional and optimized DSPRO processes for the SGRs.

for 5M-0.6 M, 5M-1.2 M. 1.2M-0.02 M, and 0.6M-0.02 M, respectively. Therefore, a smaller membrane area for the second DSPRO stage was required in the optimized processes than the conventional ones. In accordance with the DSPRO process design demonstrated in Fig. 1, lower water flux in the optimized process requires a smaller membrane area in the second DSPRO stage. The results pointed out a 9% to 21% reduction in the second stage membrane area of the optimized processes, suggesting that Q_F optimization would reduce the capital cost of the DSPRO (Fig. 7A).

Determining the optimum value of the Q_F brought about a higher enhancement in the specific power generation than the optimization of the applied pressure or the Q_D. When the DSPRO process was operated at its optimal feed solution flow rate, the increase in specific power generation in stage one (Eo1) was 31% for 5M-0.6 M, 19% for 5M-1.2 M, 24% for 1.2M-0.02 M, and 46% for 0.6M-0.02 M (Fig. 7B). While the increase in Eo2 was 6% for 5M-0.6 M, 4% for 5M-1.2 M, 8% for 1.2M-0.02 M, and 2% for 0.6M-0.02 M. Generally, the increase in the Eo1 was higher than the increase in Eo2 due to the higher water flux in stage one compared to stage two of the DSPRO process. It is also due to the lesser osmotic power and hence water flux in stage two of the DSPRO process. The enhance in the total specific power generation (E_tot) due to Q_F optimization was 24.39%, 15.44%, 20.58% and 34.54% for 5M-0.6 M, 5M-1.2 M, 1.2M-0.02 M, and 0.6M-0.02 M, respectively. The Eo_tot in the optimized DSPRO was 0.602, 0.318, 0.193, and 0.069 kWh/m^3 for 5M-0.6 M, 5M-1.2 M, 1.2M-0.02 M, and 0.6M-0.02 M, respectively. When the DSPRO is compared to a single-stage PRO, Eo_tot was 27.6%, 30.7%, 27.1%, and 23.9% higher in the DSPRO process for 5M-0.6 M, 5M-1.2 M, 1.2M-0.02 M, and 0.6M-0.02 M, respectively.

Table 2 shows the percentage increase in Eo_tot in the DSPRO process at optimum operating conditions. The maximum increase in the specific power occurred at the optimum Q_F, followed by the optimum Q_D followed by the hydraulic pressure. As such, the systematic simulation-

Table 2
The percentage increase in total specific power generation in the DSPRO processes resulting from the systematic simulation-based optimization of the main process parameters.

Salinity gradient resources (M)	The percentage increase in the total specific power generation at an optimum applied pressure	The percentage increase in the total specific power generation at an optimum draw flow rate	The percentage increase in the total specific power generation at an optimum feed flow rate
5–0.6	0.007%	9.10%	24.39%
5–1.2	0.022%	13.93%	15.44%
1.2–0.02	0.025%	8.05%	20.58%
0.6–0.02	2.45%	24.22%	34.54%

Table 3
The optimum values of applied pressure and draw solution flow rate at the systematic simulation-based optimization of the DSPRO process with the maximum percentage of the specific power generation.

SGR (M)	The Optimum Values of P (bar)	The Optimum Values of Q_D (L/h)
5–0.6	108	570
5–1.2	93.83	487
1.2–0.02	29.15	569
0.6–0.02	16.13	367

based optimization of the Q_F at the optimum values of the applied pressure and the Q_D rate is considered next to determine the percentage increase in Eo_tot due to the systematic simulation-based optimization in the DSPRO processes for the SGRs.

3.6. Optimization of feed flow rate at optimum draw flow rate and pressure

This section obtains the optimum draw solution flow rate and hydraulic pressure parameters from the simulation processes mentioned above (Table 3) to optimize the Q_F. The Q_F/Q_D ratio, A_2/A_1 ratio, and Eo_tot of the optimized and conventional DSPRO processes are shown in Fig. 8. The Q_F/Q_D ratio increases with raising water flux to overcome the impact of concentrative CP. It also relies on the nature of SGR that determines water flux in the membrane. For example, the Q_F/Q_D ratio increased from 35.11% for 5M-1.2 M SGR to 46.32% for 5M-0.6 M SGR due to the greater permeation flux in the latter salinity gradient. This observation was also found in 1.2M-0.02 M and 0.6M-0.02 M SGRs. A higher Q_F/Q_D ratio is required in the 0.6M-0.02 M salinity gradient to overcome the impact of CP when using a low concentration draw solution such as seawater (0.6 M). The membrane area in stage two was larger in the optimized process than the conventional process (Fig. 8A) due to the lower Q_D in the first DSPRO stage (Eq. (11)). A_2/A_1 ratio of the optimized processes was 33.81%, 25.54%, 41.96%, and 36.64% for 5M-0.6 M, 5M-1.2 M, 1.2M-0.02 M, and 0.6M-0.02 M, respectively. While A_2/A_1 ratio of the conventional processes was 24.9%, 16.34%, 33.53%, and 23.57% for 5M-0.6 M, 5M-1.2 M, 1.2M-0.02 M, and 0.6M-0.02 M, respectively.

The Eo_tot was higher in the optimized DSPRO processes than the conventional processes (Fig. 8B). Although a significant enhancement in Eo_tot was achieved in the optimized processes, the increase in Eo_tot was higher in the first DSPRO stage. It could also be related to the greater permeation flow in the first DSPRO stage compared to the second DSPRO stage. The osmotic pressure in the second DSPRO stage was lower than in the first stage, leading to a lower water flux. The maximum increase in Eo_tot due to the optimization was 133.54% for 0.6M-0.02 M, followed by 108.8% for 5M-1.2 M, 71.07% for 5M-0.6 M, and 63.18% for 1.2M-0.02 M. Results in Fig. 8B reveal that using a low concentration feed solution, such as 0.02 M wastewater, would improve the optimized DSPRO process due to the negligible internal CP on the feed solution side.

The outcomes revealed the advantages of DSPRO over the single-stage PRO process in rising the energy output from salinity gradient resources. There was a considerable enhancement in the specific power generation in the DSPRO processes with 5M-0.6 M, 5M-1.2 M, and 0.6M-0.02 M SGRs. Fig. 8 revealed that Eo_tot increased by 22% when a second PRO process was added. The increase in the energy output due to adding a second PRO stage was 21.5%, 19.1%, 22.4%, and 20.5% for 5M-0.6 M, 5M-1.2 M, and 0.6M-0.02 M salinity gradient resources, respectively. This underlines the benefit of using the DSPRO process compared to the single PRO process regarding renewable power generation. Moreover, this may encourage the development and usage of hybrid systems where DSPRO can be coupled with desalination units as RO to reduce the power consumption and minimize the water pretreatment steps [4].

3.7. Mass transfer, solute resistivity and pressure drop impact on DSPRO performance

The previous DSPRO simulation scenarios considered the impact of hydrodynamic conditions on the k_d and the K along the full-scale PRO module. Three scenarios are investigated here to study the DSPRO process performance

i Case 1 assumes k_d and K are variables with pressure drop in the PRO module
ii Case 2 assumes k_d and K are constants with pressure drop in the PRO module
iii Case 3 assumes k_d and K are without pressure drop in the PRO module

In the comparison study, case 1 vs case 2 displays the effect of k_d and K, case 2 vs case 3 displays the effect of pressure drop, and case 3 vs case 1 shows the effect of k_d, K, and pressure drop on the process performance (Table 4).

The results were obtained at 1000 L/h feed and draw solutions flow rates and a hydraulic pressure equal to $\pi/2$ to determine the impact of these parameters under the same experimental conditions. Fig. 9 explains the specific power generation in the first and second stages (Eo1 and Eo2), total specific power generation (E_tot), and A_2/A_1 ratio in DSPRO processes. In the first DSPRO stage, the specific power generation for 5M-0.6 M was 0.361, 0.360, and 0.359 kWh/m^3 in case 1, case 2, and case 3, respectively. The results indicated that the DSPRO performance was subtly higher in case 1 (Fig. 9A). The same trend was noticed for 5M-1.2 M and 1.2M-0.02 M (Fig. 9B and 9C), in which Eo1 was the highest in case 1. For 0.6M-0.02 M, Eo1 was slightly higher (0.0382 kWh/m^3) in case 3 (Fig 9.D) as a consequence of the combined impact of the applied pressure and water flux on the specific power generation (Fig. A3B-Appendix A). In the second DSPRO stage, the maximum specific power generation was in case 2, followed by case 3, then case 1 for 5M-0.6 M, 5M-1.2 M, and 1.2M-0.02 M. Compared to case 2, there was 11.14%, 13.04%, 9.2%, and 8.82% reduction in the second stage power generation for 5M-0.6 M, 5M-1.2 M, 1.2M-0.02 M, and 0.6M-0.02 M, respectively, due to changing k_d and K in case 1. The increase in Eo2 in case 2 was due to increasing the permeation flux in stage 2 (Fig. A2-Appendix A). Nevertheless, the highest increase in Eo2 for 0.6M-0.02 M was in case 3 (Fig. 9D). The difference in the specific power generation of the DSPRO at constant k_d and K and ignoring the effect of pressure drop in the membrane is af-

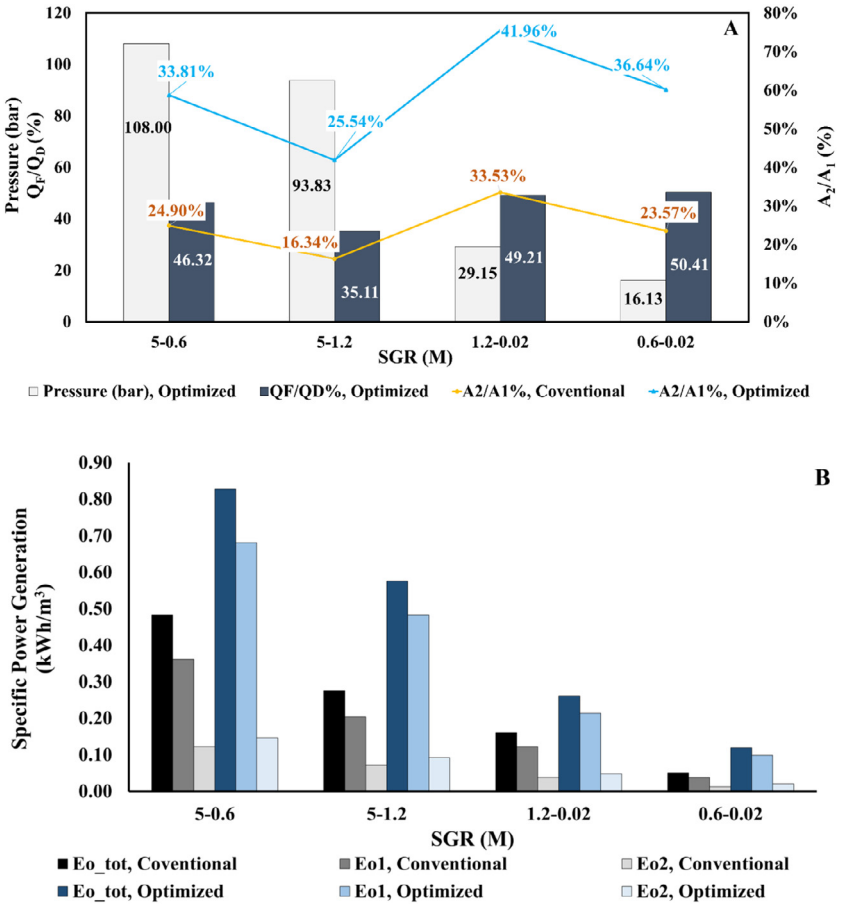

Fig. 8. The optimum feed solution flow rate at the optimum applied pressure values and the draw flow rates of the DSPRO process on the produced power generation for various SGRs. A: the conventional and optimized ratio of Q_F/Q_D% and the conventional and optimized ratio of A_2/A_1% for the four SGRs. B: Eo1, Eo2, and Eo_tot in the conventional and optimized DSPRO processes for the SGRs.

Table 4
The effect of considering the variation of k_d, K and the pressure drop along membrane modules in the DSPRO processes for the SGRs in the total specific power generation.

Scenarios	Parameters	SGRs NaCl (M)	Comparison	% Difference in Eo1	% Difference in Eo2	%Difference in Eo_tot
Case 1	k_d and K are variables with pressure drop	5–0.6	Case 1 Vs. Cas2	0.39	−11.14	−2.8
		5–1.2		0.57	−13.04	−3.37
		1.2–0.02		0.78	−9.2	−1.78
		0.6–0.02		0.39	−8.82	−2.13
Case 2	k_d and K are constants with pressure drop	5–0.6	Case 2 Vs. Case 3	0.25	1.66	0.63
		5–1.2		0.25	1.07	0.49
		1.2–0.02		1.04	5.98	2.27
		0.6–0.02		−0.79	−1.63	−1.03
Case 3	k_d and K are constants without pressure drop	5–0.6	Case 3 Vs. Case 1	−0.63	10.7	2.24
		5–1.2		−0.81	13.77	2.99
		1.2–0.02		−1.8	3.92	−0.44
		0.6–0.02		0.41	11.49	3.23

fected by water flux and hydraulic pressure. For 0.6M-0.02 M SGR, water flux was higher in case 1 than in case 3 (Fig. A2D-Appendix A), but Eo2 was higher in case 3 in which the pressure drop was ignored due to the higher hydraulic pressure (Fig. A3B-Appendix A). For 5M-0.6 M, 5M-1.2 M, and 1.2M-0.02 M, Eo_tot was greater in case 2 than in case 1. Compared to in case 2, Eo_tot decreased by 2.8%, 3.37%, 1.78%, and 2.13% for 5M-0.6 M, 5M-1.2 M, 1.2M-0.02 M, and 0.6M-0.02 M, respectively, in case 1. Comparing case 3 to case 1, 2.24%, 2.99%, and 3.23% increase in the Eo_tot occurred for 5M-0.6 M, 5M-1.2 M, and 0.6M-0.02 M, respectively, due to the variation in k_d, K, and considering the pressure drop in the modules. In contrast, a reduction of 0.44% for 1.2M-0.02 M (Table 4) occurred due to the reduction in the permeation flow and applied pressure in case 1 compared to case 3 (Fig. A3A-Appendix).

There was also a subtle difference in the A_2/A_1 ratio in case 1, case 2, and case 3. A_2/A_1 ratio was slightly higher in the DSPRO processes performed in case 1 followed by case 2, then case 3 as a result of the greater permeation flow rate in stage one (Fig. A2-Appendix A). A_2 is influenced by the permeate flow rate (Eq. (11)); the higher the permeation rate in the first DSPRO stage, the higher A_2/A_1 ratio. The variation of k_d, K, and considering the pressure drop in the membrane generated a higher permeation flow rate in stage one, which forms the draw solution flow rate in stage two, increasing the membrane area of stage two.

Practically, k_d and K parameters and the pressure drop will change in the full-scale module due to the variation in feed and draw solution flow rates. Overlooking variation in k_d and K parameters will overestimate Eo_tot, as shown in case 2 relative to case 1. Likewise, ignoring the pressure drop along the PRO membrane will subtly affect Eo_tot, as

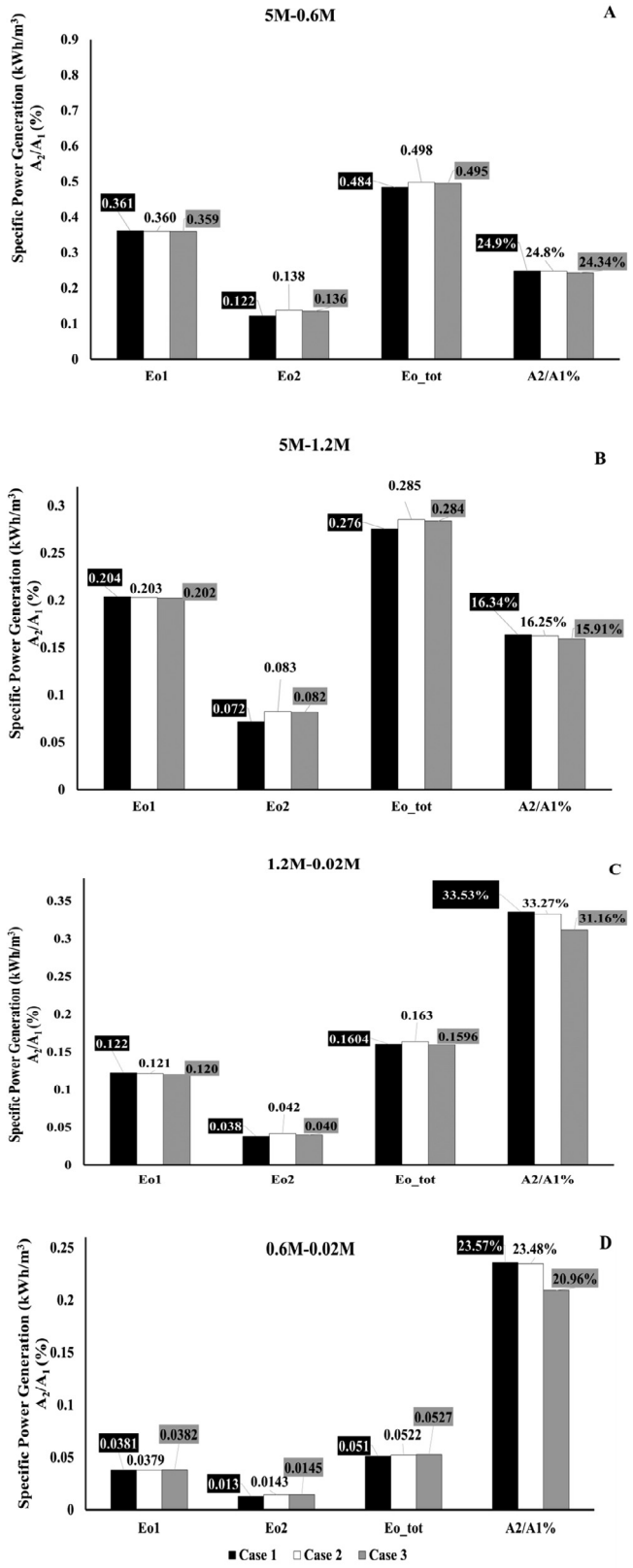

Fig. 9. The impact of changing k_d and K and included the pressure drop in the DSPRO processes on the produced power generation in the first, second stages and the total amount at case 1, case 2, and case 3 on 5M-0.6 M, 5M-1.2 M, 1.2M-0.02 M, and 0.6M-0.02 M (A, B, C, and D, respectively).

shown in case 3 compared to case 2. Overall, results in Fig. 9 showed the impact of k_d and K parameters on Eo_tot (case 1 vs case 2) is higher than the impact of pressure drop on the Eo_tot (case 2 vs case 3). In effect, the DSPRO performance would be closer to real field conditions when pressure drop and variation in hydrodynamic conditions are included in calculating the specific power generation.

4. Conclusion

DSPRO process was suggested for higher power generation from SGRs. However, the determination of the optimum operating parameters would further enhance process performance. Process systematic simulation would improve the produced specific energy and lower the cost of energy required. The study results revealed that the optimum ratio of the QF/QD is lower than that in the conventional processes. Additionally, the results indicated that the feed solution flow rate is the most influential parameter affecting the performance of the DSPRO process, followed by the draw solution flow rate and hydraulic pressure. The DSPRO process total power generation could be increased by 71.07%, 108.8%, 63.18%, and 133.54% for DS-SW, DS-ROB, ROB-WW, and SW-WW SGRs, respectively, after optimizing the operating parameters. For the first time, the study evaluated the impact of hydrodynamic parameters, such as k_d and K coefficients, in process simulation. The study found that k_d and K coefficients affect the DSPRO process performance, and overlooking these parameters may overestimate the total specific power generation in the DSPRO process. This study showed 2.8% more power generation occurred in the DSPRO process using DS-SW SGR when k_d and K were considered constants. Moreover, the total power generation was increased by 0.63% for DS-SW when the pressure drop was ignored in the DSPRO process while ignoring k_d and K variations and pressure drop in the process results in 2.24% higher energy output. Accordingly, the results showed that k_d and K variations in the DSPRO process would have more impact than ignoring pressure drops on the energy output. These parameters should be considered in estimating the energy produced from an SGR.

Declaration of Competing Interests

The authors declare that they have no known competing financial interests or personal relationships that could have appeared to influence the work reported in this paper.

Acknowledgement

The authors wish to express their gratitude for the assistance provided by an Australian Government Research Training Program Scholarship.

Appendix A

A.1. The impact of the optimum hydraulic pressure

Water flux of the DSPRO process declines through the membrane modules due to the lessening of the osmotic power through the membrane length. In the second DSPRO stage, the water flux increased as the osmotic power increased by the fresh feed solution due to adding new feed to that stage. Determination of the optimum value of the applied pressure in the DSPRO process showed mitigation in the water flux for 5M-1.2 M SGR (Fig. A1). The optimum applied pressure was greater than the applied pressure in the conventional DSPRO process, causing a reduction in the amount of water permeating through the membrane modules in the DSPRO both stages, which explains the reduction in the water flux due to the usage of the optimum hydraulic pressure.

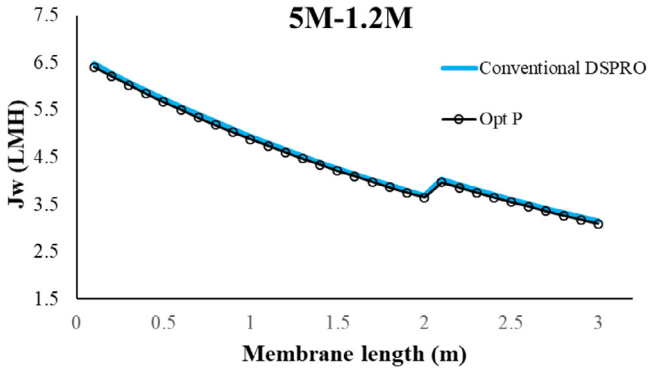

Fig. A1. Water flux along the membrane modules in the DSPRO process where two modules in stage one and one module in stage two for 5M-1.2 M SGR. $P_{Di,1}$ is 92.57 bar and equal flow rates of 1000 L/h of the feed and the draw solutions in the conventional case. While $P_{Di,1}$ is 93.83 bar at 1000 L/h feed flow rate and 1000 L/h draw flow rate for the DSPRO process at optimum pressure.

A.2. The impact of variation of mass transfer, solute resistivity and pressure drop on water flux

The impact of variation in mass transfer, solute resistivity and pressure drop through the membrane modules in DSPRO processes was considered for 5M-0.6 M, 5M-1.2 M, 1.2M-0.02, and 0.6M-0.02 M. Fig. A2 represents the variation in the water flux along the membrane modules of the DSPRO processes performed at case 1, case 2, and case 3 for all SGRs. For all SGRs; higher water flux in the first DSPRO stage was obtained at case 1 followed by case 2 than case 3, which means that considering the variation in k_d, K, and the pressure drop in the DSPRO processes improve the water permeation through the membrane in the first DSPRO stage. Higher water flux at the second DSPRO stage performed at case 2 resulted from all SGRs, representing that ignoring the variation of kd and K along the DSPRO membrane modules will overestimate the water flux in the second DSPRO stage. Ignoring the pressure drop at the DSPRO processes performed in case 3 displayed lower water flux for all SGRs than the water flux of the DSPRO processes performed in case 2. The figure shows that the water flux is affected by k_d, K, and the pressure drop in the DSPRO processes for all SGRs, and their impacts cannot be ignored.

A.3. The impact of variation of mass transfer, solute resistivity and pressure drop on permeation rate and the hydraulic pressure

As discussed earlier, the variation of k_d, K, and the pressure drop affect the DSPRO process's performance represented by the specific power generation. The applied hydraulic pressure controls the specific power generation, permeation flow rate, feed, and draw solutions flow rates. Since the feed and the draw solutions flow rates are the same for all the cases presented in Section 3.7; then the variation in specific power generation between the SGRs was governed by the permeation flow rate and the applied hydraulic pressure. Accordingly, the combined effect of the permeation rate (Qp) and the applied hydraulic pressure (P) was studied and shown in Fig. A3. The figure shows the permeate flow rate times the applied pressure for the DSPRO processes of 1.2M-0.02 M and 0.6M-0.02 M performed at case 1 and case 3. Qp*P is higher for the DSPRO process performed at case 1 for 1.2M-0.02 M than case 3. The water flux of the DSPRO process of 1.2M-0.02 M performed at case1 showed higher values than the water flux of the DSPRO process performed in case 3 (Fig. A2C-Appendix). For the DSPRO process performed in case 3, the pressure drop was ignored, then the optimum applied pressure was higher than the DSPRO process performed in case 1.

Nevertheless, the combined effect of the lower permeate flow rate and higher applied pressure caused a reduction in Qp*P for the DSPRO process at case 3 compared to case 1, which clarifies that Eo_tot for the DSPRO process of 1.2M-0.02 M was lower in case 3 relative to the case 1 (Fig. 9C). The scenario was the opposite of the DSPRO process of 0.6M-0.02 M. Qp*P is lower for the DSPRO process performed at case 1 for 0.6M-0.02 M than case 3. The water flux of the DSPRO process of 0.6M-0.02 M performed at case1 showed higher values than the water flux of the DSPRO process performed in case 3 (Fig. A2D-Appendix). For the DSPRO process performed in case 3, the pressure drop was ignored,

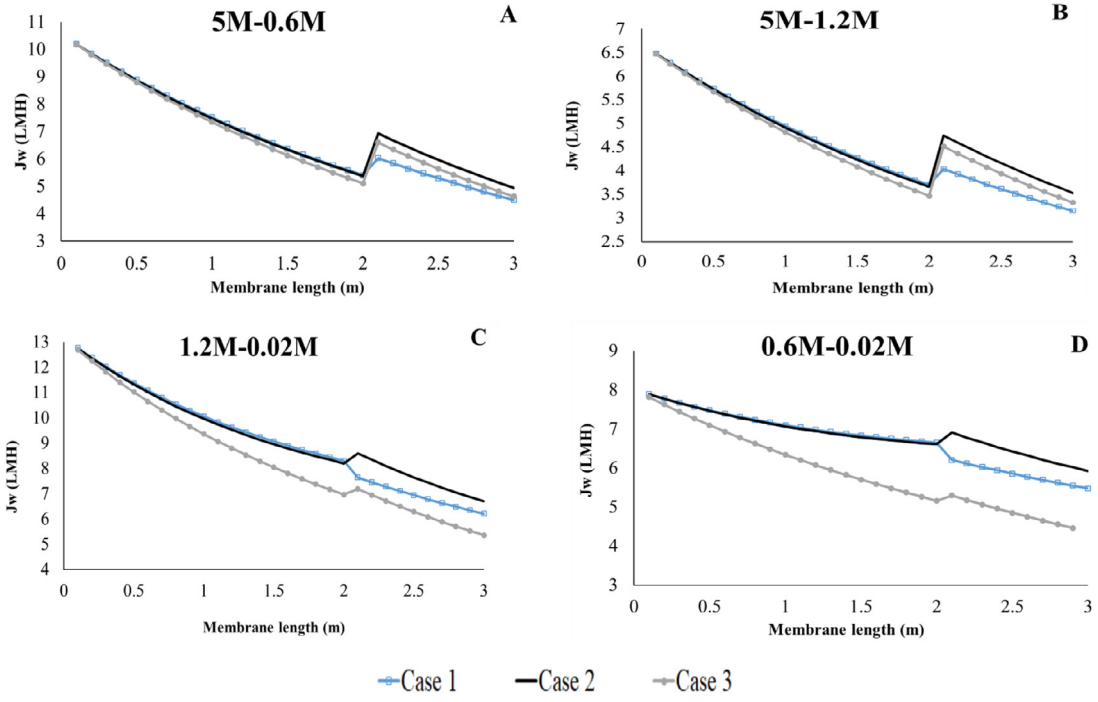

Fig. A2. The variation in the water flux along the membrane modules in the DSPRO processes performed at case 1, case 2, and case 3 for 5M-0.6 M (figure A), 5M-1.2 M (figure B), 1.2M-0.02 M (figure C), and 0.6M-0.02 M (figure D).

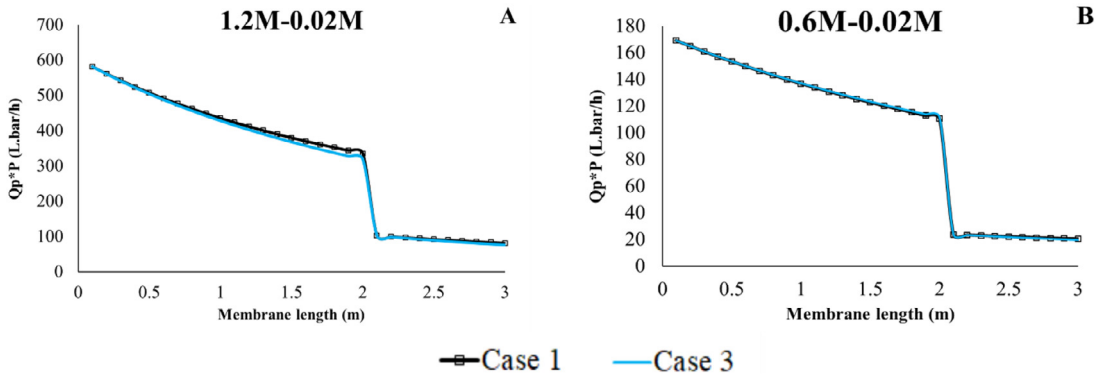

Fig. A3. The variation in the permeate flow rate along the membrane modules in the DSPRO processes performed at case 1 and case 3 for 1.2M-0.02 M (figure A) and 0.6M-0.02 M (figure B).

then the optimum applied pressure was higher than the DSPRO process performed in case 1. Then, the combined effect of the lower permeate flow rate and higher applied pressure caused enhancement in Qp*P for the DSPRO process in case 3 relative to the case 1, which explains that Eo_tot for the DSPRO process of 0.6M-0.02 M was higher in case 3 relative to the case 1 (Fig. 9D).

References

[1] U. Shahzad, The need for renewable energy sources, ITEE J. 15 (2012) 16–18.

[2] N. Nakicenovic, in: A.P.P. Thomas, B. Johansson, Nebojša Nakićenović, Luis Gomez-Echeverri (Eds.), *Renewable Energy* in *Global Energy Assessment: Toward a Sustainable Future*, Cambridge University Press, 2012, pp. 767–900. Editor2012.

[3] Hyung Won Chung, Jaichander Swaminathan, J.H.L. V, Multistage pressure-retarded osmosis configurations: a unifying framework and thermodynamic analysis, Desalination (2019) 476, doi:10.1016/j.desal.2019.114230.

[4] Nahawand AlZainati, et al., Pressure retarded osmosis: advancement, challenges and potential, J. Water Process. Eng. 40 (2021), doi:10.1016/j.jwpe.2021.101950.

[5] Wei He, Yang Wang, M.H. Shaheed, Enhanced energy generation and membrane performance by two-stage pressure retarded osmosis (PRO), Desalination 359 (2015) 186–199, doi:10.1016/j.desal.2014.12.014.

[6] Ali Altaee, et al., Evaluation the potential and energy efficiency of dual stage pressure retarded osmosis process, Appl. Energy 199 (2017) 359–369, doi:10.1016/j.apenergy.2017.05.031.

[7] Sung Ho Chae, J.H. Kim, *Integration of PRO into desalination processes*„ Pressure Retarded Osmosis (2017) 129–151.

[8] Roghayeh Soltani, H. Struchtrup, Modeling and simulation of the dual stage pressure retarded osmosis systems, Desalination 460 (2019) 28–40, doi:10.1016/j.desal.2019.02.010.

[9] Ali Altaee, Andrea Cippolina, Modelling and optimization of modular system for power generation from a salinity gradient, Renew. Energy 141 (2019) 139–147, doi:10.1016/j.renene.2019.03.138.

[10] Shenhan Wang, et al., Analysis and optimization of dual-stage pressure retarded osmosis for renewable power generation, Chem. Eng. Trans. 61 (2017) 1813–1818, doi:10.3303/CET1761300.

[11] A. Altaee, et al., Limitations of osmotic gradient resource and hydraulic pressure on the efficiency of dual stage PRO process, Desalination Water Treat 105 (2018) 11–22, doi:10.5004/dwt.2018.22128.

[12] Masaru Kurihara, M. Hanakawa, Mega-ton water system: Japanese national research and development project on seawater desalination and wastewater reclamation, Desalination 308 (2013) 131–137, doi:10.1016/j.desal.2012.07.038.

[13] Esther Swin Hui Lee, et al., A pilot study on pressure retarded osmosis operation and effective cleaning strategies, Desalination 420 (2017) 273–282, doi:10.1016/j.desal.2017.08.004.

[14] Yingxue Chen, et al., Optimization of module pressure retarded osmosis membrane for maximum energy extraction, J. Water Process. Eng. 32 (2019), doi:10.1016/j.jwpe.2019.100935.

[15] Adnan Alhathal Alanezi, A. Altaee, Enhanced performance dual stage pressure retarded osmosis, Energy Procedia 142 (2017) 4182–4197, doi:10.1016/j.egypro.2017.12.344.

[16] Ali Altaee, et al., Dual stage PRO process: impact of the membrane materials of the process performance, Desalin. Water Treat 57 (14) (2015) 1–12, doi:10.1080/19443994.2015.1007173.

[17] Habtom TekluAseffa, Dinesh KumarGautam, Senthilmurugan Subbiah, Optimization of pressure retarded osmosis process and estimation of Indian blue energy capacity, Desalination 498 (2021), doi:10.1016/j.desal.2020.114752.

[18] Ali Altaee, Guillermo Zaragoza, A. Sharif, Pressure retarded osmosis for power generation and seawater desalination: performance analysis, Desalination 344 (2014) 108–115, doi:10.1016/j.desal.2014.03.022.

[19] Shihong Lin, Anthony P. Straub, M. Elimelech, Thermodynamic limits of extractable energy by pressure retarded osmosis, Energy Environ. Sci. 7 (2014) 2706–2714, doi:10.1039/c4ee01020e.

[20] S. Senthil, S. Senthilmurugan, Reverse osmosis–pressure retarded osmosis hybrid system: modelling, simulation and optimization, Desalination 389 (2016) 78–97, doi:10.1016/j.desal.2016.01.027.

[21] Hegazy Rezk, Ahmed Fathy, A.Y. Abdelaziz, A comparison of different global MPPT techniques based on meta-heuristic algorithms for photovoltaic system subjected to partial shading conditions, Renew. Sust. Energ. Rev. 74 (2017) 377–386, doi:10.1016/j.rser.2017.02.051.

[22] Henrik T. Madsen, et al., Pressure retarded osmosis from hypersaline solutions: investigating commercial FO membranes at high pressures, Desalination 420 (2017) 183–190, doi:10.1016/j.desal.2017.06.028.

[23] H. Joseph Kestin, Ezzat Khalifa, R.J. Correia, Tables of the dynamic and kinematic viscosity of aqueous NaCl solutions in the temperature range 20–150 °C and the pressure range 0.1–35 MPa, J. Phys. Chem. Ref. Data 10 (71) (2009) DOI:, doi:10.1063/1.555641.

[24] V.M.M. LOBO, Mutual diffusion coefficients in aqueous electrolyte solutions, Pure & Appl. Chern. 65 (12) (1993) 2613–2640.

[25] Ali Altaee, et al., Pressure retarded osmosis process for power generation: feasibility, energy balance and controlling parameters, Appl. Energy 206 (2017) 303–311, doi:10.1016/j.apenergy.2017.08.195.

[26] Ali Altaee, et al., Single and dual stage closed-loop pressure retarded osmosis for power generation: feasibility and performance, Appl. Energy 191 (2017) 328–345, doi:10.1016/j.apenergy.2017.01.073.

[27] Andrea Achilli, Tzahi Y. Cath, A.E. Childress, Power generation with pressure retarded osmosis: an experimental and theoretical investigation, J. Membr. Sci. 343 (1–2) (2009) 42–52, doi:10.1016/j.memsci.2009.07.006.

[28] N.H. Sarper Sarp, Thermodynamic optimization of multistage pressure retarded osmosis (MPRO) with variable feed pressures for hypersaline solutions, Desalination 477 (2020) 114245.

[29] R.A. Tufa, et al., *3.8 Membrane-based processes for sustainable power generation using water: pressure-retarded osmosis (PRO), reverse electrodialysis (RED), and capacitive mixing (CAPMIX)*, in, Comprehens Membrane Sci Eng (2017) 206–248.